JOURNAL OF GEOPHYSICAL RESEARCH, VOL. 112, D13106, doi:10.1029/2006JD007654, 2007

Decadal changes of ENSO persistence barrier in SST and ocean heat content indices: 1958–2001

Jin-Yi Yu[1] and Hsun-Ying Kao[1]

Received 14 June 2006; revised 31 October 2006; accepted 14 January 2007; published 4 July 2007.

[1] Decadal changes of El Niño-Southern Oscillation (ENSO) persistence barriers in various indices of sea surface temperature (SST) and ocean heat content (OHC) are examined in this study using observations and ocean data assimilation products for the period 1958–2001. It is found that the SST indices in the eastern and central equatorial Pacific exhibit very different decadal barrier variability. The variability is large for the eastern Pacific SST indices (NINO1+2 and NINO3) whose persistence barriers shifted abruptly in 1976/1977 and 1989/1990. In contrast, the central Pacific SST indices (NINO3.4 and NINO4) experienced little decadal barrier variability and have had their persistence barriers fixed in spring in the past four decades. The zonal mean OHC index averaged over the equatorial Pacific shows decadal barrier changes similar to those in the eastern Pacific SST indices and always leads the NINO3 SST barrier by about one season. It is noticed that the SST persistence barrier appeared first in the eastern Pacific before 1976/1977, first in the central Pacific between 1976/1977 and 1989/1990, and almost simultaneous in both the eastern and central Pacific after 1989/1990. These timings coincide with the westward propagating, eastward propagating, and standing pattern of ENSO SST anomalies observed in these three periods. These results suggest that ENSO SST anomalies in the equatorial Pacific can be considered to consist of two different processes: a central Pacific process whose phase transition (such as onset) and barrier always happen in spring, and an eastern Pacific process whose phase transition and barrier change from decade to decade and are influenced by changes in the mean thermocline depth along the equatorial Pacific.

Citation: Yu, J.-Y., and H.-Y. Kao (2007), Decadal changes of ENSO persistence barrier in SST and ocean heat content indices: 1958–2001, *J. Geophys. Res.*, *112*, D13106, doi:10.1029/2006JD007654.

1. Introduction

[2] El Niño-Southern Oscillation (ENSO), a prominent climate phenomenon in the coupled ocean-atmosphere system of the tropical Pacific, has great impacts on the global climate. Extended-range forecasts of ENSO have obtained encouraging success over the past decade [*Latif et al.*, 1998]. It was noticed that ENSO predictions tend to be less successful if the forecasts are launched before and through the spring [*Barnston et al.*, 1994]. This low predictability has been related to the so-called spring persistence barrier of ENSO, which refers to the weak persistence of ENSO anomalies in the boreal spring. Lagged autocorrelation analyses with various ENSO indices, such as NINO3 (5°S–5°N; 150°–90°W) sea surface temperature (SST) anomalies, Southern Oscillation pressure differences, and central Pacific rainfall anomalies, show sharp declines in the autocorrelation coefficients in spring [*Troup*, 1965; *Wright*, 1979; *Webster and Yang*, 1992; *Torrence and Webster*, 1998; *Clarke and Van Gorder*, 1999]. Recently, *McPhaden* [2003] showed that the persistence barrier of subsurface ocean temperature (i.e., the ocean heat content—OHC) anomalies of ENSO occurs in a different season. He analyzed a warm-water volume index which is defined as the observed volume of water between the surface and the 20°C isotherm in the equatorial Pacific during the period of 1980–2000 and showed that the persistence barrier of this OHC index occurred in winter. The OHC index has the strongest persistence in the spring when the persistence of NINO3 SST anomalies is the weakest. Because of this phase lag, the strong persistence of OHC offsets the spring persistence barrier of SST and offers a possible avenue to improve long-term ENSO prediction. *McPhaden* [2003] argued that this helps explain why ENSO forecasts are improved when the subsurface ocean data (or more accurate wind forcing, which affects subsurface ocean structure) are utilized in the forecast models [e.g., *Chen et al.*, 1995; *Xue et al.*, 2000].

[3] Several ENSO properties, such as amplitude, frequency, and propagation, are known to change from decades to decades [e.g., *Gu and Philander*, 1995; *Wang*, 1995; *Torrence and Webster*, 1998; *An and Wang*, 2000; among others]. Earlier studies have examined and noticed decadal variations in the

[1]Department of Earth System Science, University of California, Irvine, California, USA.

0148-0227/07/2006JD007654$09.00

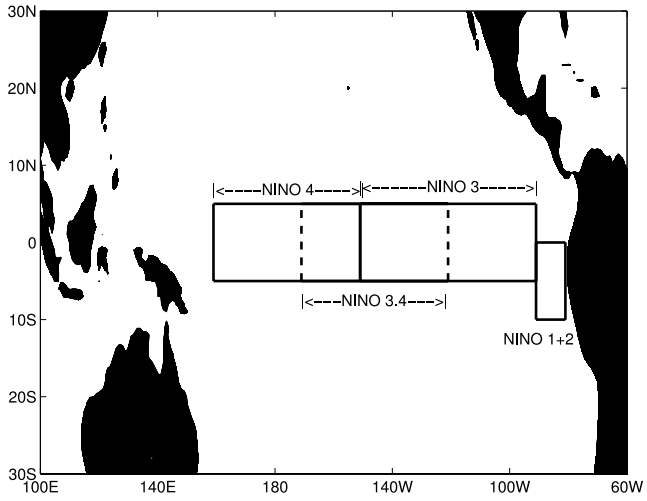

Figure 1. Areas covered by the NINO1+2, NINO3, NINO3.4, and NINO4 SST indices.

persistence barriers of the NINO3 SST and SOI pressure indices [*Balmaseda et al.*, 1995; *Torrence and Webster*, 1998; *Weiss and Weiss*, 1999; *Clarke and Van Gorder*, 1999]. *Balmaseda et al.* [1995] concluded that the spring SST barrier was strong in the 1970s but weak in the 1980s. However, the decadal variability in the persistence barrier of ENSO OHC anomalies has not been examined. It is not known if the decadal change of the OHC barrier coincides with the change of the SST barrier and if the phase lag between these two barriers remains the same as ENSO properties change from decade to decade. If the phase lag changes on decadal timescales, the OHC information may not always be helpful for improving ENSO predictions, and new forecasting techniques that better incorporate subsurface information may have to be developed.

[4] The objective of this study is to analyze reanalysis and assimilation data available from the past four decades (1958–2001) to determine the decadal changes of ENSO persistence barriers in OHC and SST and their lag relations. For the SST barrier, most earlier studies focused on the NINO3 SST index. In this study we also analyze the persistence barrier in other parts of the equatorial Pacific where ENSO SST anomalies occur, including NINO1+2 (0°–10°S; 80°–90°W), NINO3.4 (5°S–5°N; 170°–120°W), and NINO4 (5°S–5°N; 160°E–150°W), and compare their decadal changes to those of the NINO3 region. Figure 1 shows the locations of these NINO index regions.

[5] This paper is structured as follows. Section 2 describes the data used for the analysis. Section 3 presents the decadal variations in the persistence of ENSO OHC and NINO3 indices and their phase relations. Section 4 examines the barrier changes in all NINO regions. Section 5 links these decadal changes to the changes in the mean atmospheric and oceanic states of the equatorial Pacific region. Our conclusions and their implications are summarized in section 6.

2. Data

[6] Forty-four years (1958–2001) of monthly values of OHC, SST, surface wind are analyzed in this study. Here the

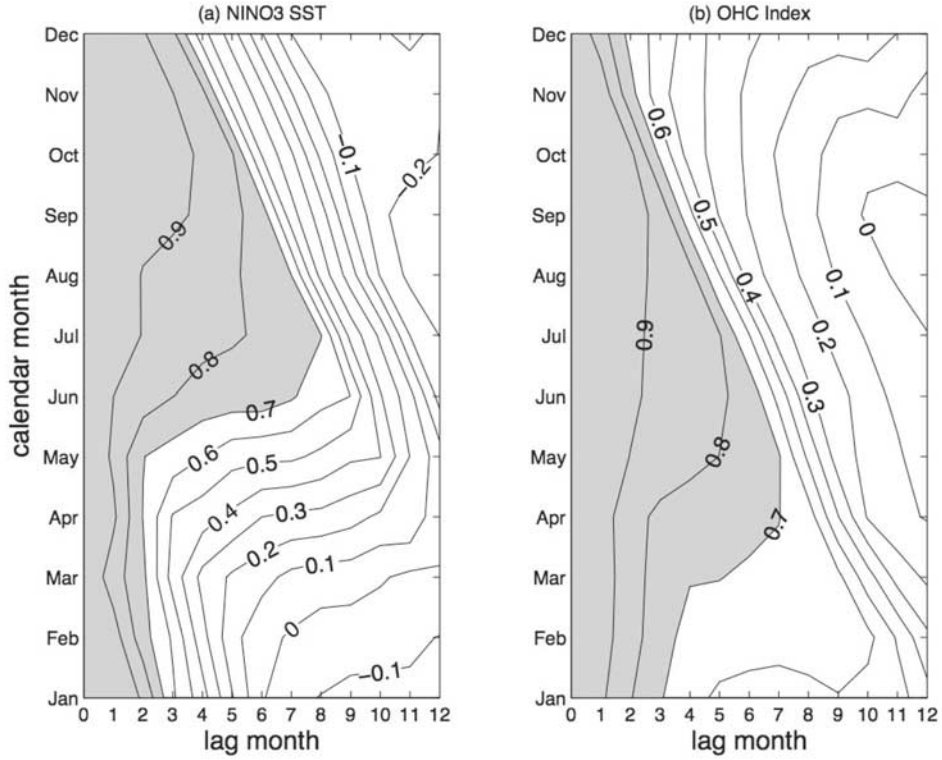

Figure 2. Lagged autocorrelation coefficients of monthly anomalies in (a) NINO3 SST and (b) zonal mean OHC as a function of starting calendar month and lag time. The calculations are performed for 1958–2001.

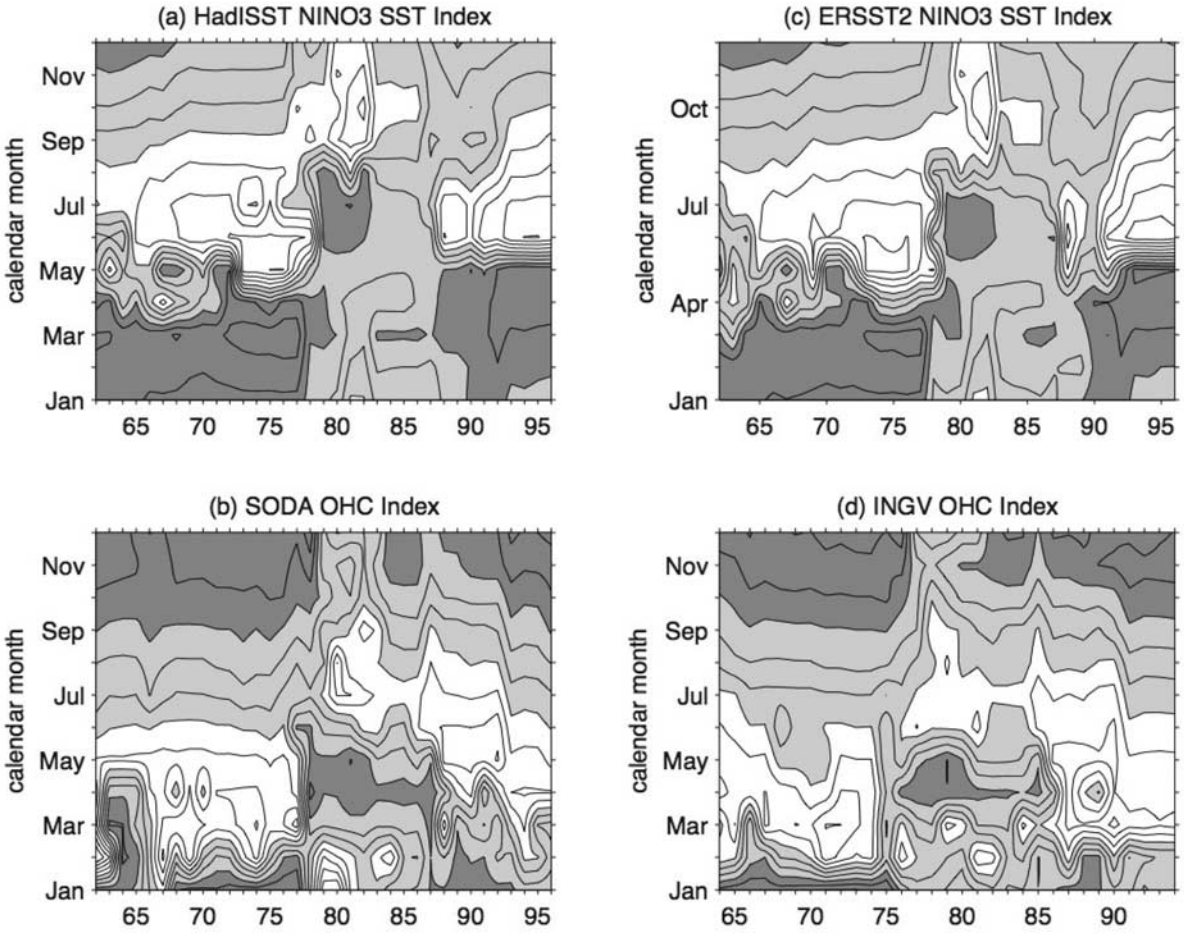

Figure 3. The lag time (in months) that the lagged autocorrelation coefficient calculated from (a) GISST NINO3 SST, (b) SODA zonal mean OHC, (c) ERSST V.2 NINO3 SST, and (d) ENACT-INGV zonal mean OHC within a 10-year moving window decrease to 0.7. The 10-year window is shifted year by year from 1958 to 2001. The dark regions indicate the years and the calendar months when the lag time is shorter than 3 months (i.e., a persistence barrier). The white regions indicate the years and months when the lag time is longer than 6 months (high persistence). The light regions have lag time between 3 and 6 months. Contour intervals are 1 month.

OHC is defined as the ocean temperatures averaged in the upper 300 m. The OHC information is calculated from the Simple Ocean Data Assimilation (SODA; *Carton et al.*, 2000a, 2000b) for 1958–2001, which is assimilated by the Parallel Ocean Program model with the atmospheric forcing from the ERA-40 atmospheric analysis [*Uppala et al.*, 1999]. The assimilation data set has 40 levels in the subsurface ocean divided unevenly from 5 to 5374 m. It covers global oceans from 75.25°S to 89.25°N with a horizontal resolution of $0.5^\circ \times 0.5^\circ$. The NINO SST indices analyzed here are calculated from the $1^\circ \times 1^\circ$ Global Sea Ice Coverage and Sea Surface Temperature (GISST) data set [*Rayner et al.*, 1996]. Two additional OHC and SST data sets are used to verify results obtained from SODA and GISST. The alternate OHC data set is the ocean analysis produced by Istituto Nazionale di Geofisica e Vulcanologia (National Institute for Geophysics and Volcanology; INGV) of Italy for European Union project "Enhanced Ocean Data Assimilation and Climate Prediction" (Enact). The ENACT-INGV ocean analysis is assimilated by the OPA ocean general circulation model [*Madec et al.*, 1998] at a $1^\circ \times 1^\circ$ resolution and is available for 1962–2001. The alternate SST datum is the Extended Reconstructed Sea Surface Temperature V2 (ERSST V.2 [*Smith and Reynolds*, 2004]) from National Oceanic and Atmospheric Administration (NOAA), which has a horizontal resolution of $2^\circ \times 2^\circ$ and is available for 1854–2006. For the analysis of surface wind, the $2^\circ \times 2^\circ$ ERA-40 reanalysis is used. In this paper, anomalies are defined as the deviations from the mean seasonal cycle of the particular field discussed.

3. Decadal Changes in the Persistence Barriers of NINO3 and OHC Indices

[7] We used lagged autocorrelation to determine the persistence barrier of ENSO indices. Figure 2a shows the lagged autocorrelation coefficients of NINO3 SST index calculated from the entire analysis period (1958–2001). The vertical axis is the starting calendar month, whereas the horizontal axis is the lag time in months. Shaded areas are

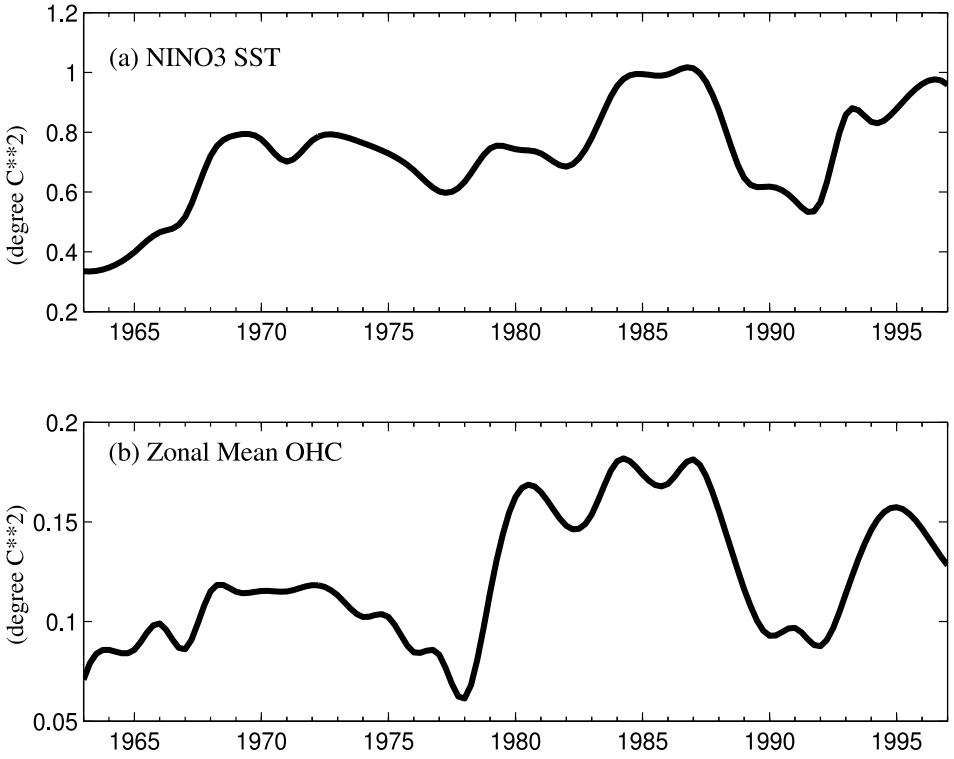

Figure 4. Variance of (a) NINO3 SST and (b) zonal mean OHC calculated within a 10-year window that moves year by year from 1958 to 2001.

correlations greater than 0.7; that is, the persistence is high. The figure shows that NINO3 SST anomalies have high persistence with the starting month in June through August. The autocorrelation coefficients remain large for the lag time up to 6–8 months. However, the coefficients drop to small values quickly with the starting month in March through May. This figure shows clearly the well-known spring persistence barrier in the NINO3 SST index. Figure 2b shows the lagged autocorrelation coefficients calculated from a zonal mean equatorial Pacific OHC index from 1958 to 2001. This index is produced by averaging OHC anomalies between 5°S and 5°N along the equatorial Pacific (120°E to 80°W). Figure 2b shows that the persistence of the OHC index in March to May is strong with the lag times of 5 to 7 months. On the contrary, the persistence is the weakest in November to January with the lag times of only 2 to 3 months. This shows that the OHC has a persistence barrier in winter, which is consistent with the barrier found by *McPhaden* [2003] for the shorter period of 1980–2000 using his warm-water volume index.

[8] To examine the decadal variation of the persistence barrier, we performed a running lagged autocorrelation analysis with the NINO3 and OHC indices. With this analysis, lagged autocorrelation coefficients are calculated within a 10-year window that is shifted gradually (by 1 year) from 1958 to 2001. Each calculation produces a lagged autocorrelation map like Figure 2. On the basis of each correlation map, the lag time (in unit of month) for which the correlation coefficient drops to 0.7 is determined for all calendar months. The value of 0.7 is subjectively chosen to characterize the persistence. The results are not sensitive to the selection of particular value for this characterization. As an example of the running analysis, assuming we calculate the lagged autocorrelation coefficients for the NINO3 SST index during a 10-year period from year a to year b and produce a lagged autocorrelation map that looks exactly like Figure 2a. From the 0.7 contour line in this figure, we can determine that the persistence of SST anomalies in year $(a + b)/2$ (the center year of the 10-year window) is 1.8 months for January, 1.5 months for February through May, 6.2 months for June, 7 months for July, . . ., and 2.6 months for December. We then shift the 10-year window forward by 1 year to cover year $a + 1$ to year $b + 1$, repeat the lagged autocorrelation calculation, and determine the SST persistence for all calendar months in year $((a +1) + (b + 1))/2$. We keep on shifting the 10-year window forward and repeat the autocorrelation calculation until the window reaches the end of the data set. We can then determine the decadal variation of persistence barrier by plotting the lag time that the coefficient drops to 0.7 (i.e., the persistence) as a function of the calendar month and the center year of the 10-year running window. Figure 3 shows the results from applying this analysis to both the NINO3 and zonal mean OHC indices. The dark shading represents the lag time shorter than 3 months and, therefore, marks the timing of low persistence (i.e., the persistence barrier). The light shading represents the lag time from 3 to 6 months. The areas without shading represent the years/months, whose lag time is longer than 6 months, and, therefore, the high persistence.

[9] In Figure 3, dramatic shifts in the timing of the persistence barrier can be identified for both ENSO indices.

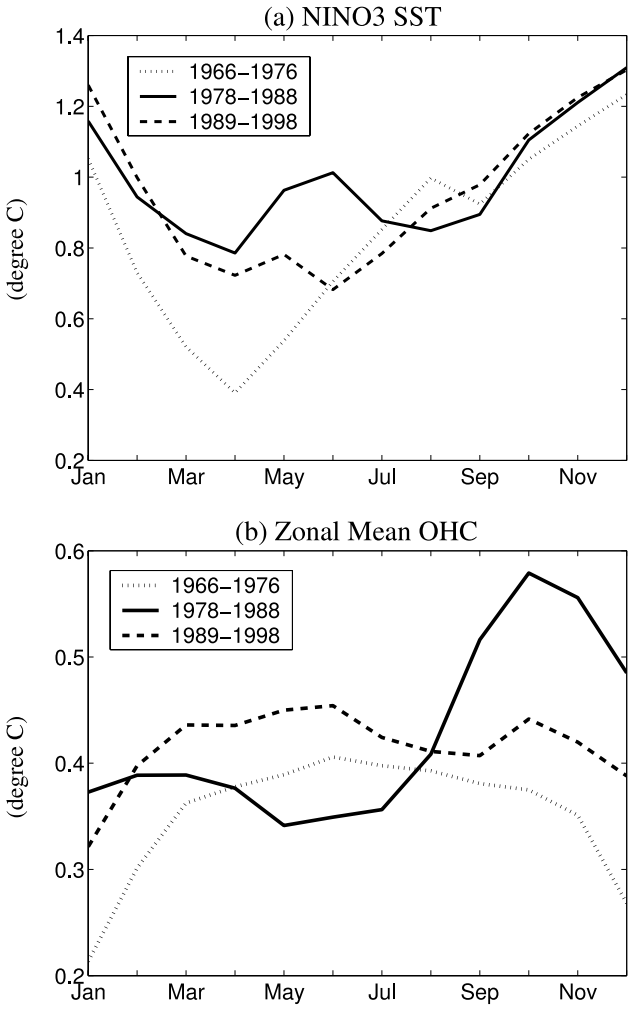

Figure 5. Standard deviations of (a) NINO3 SST and (b) zonal mean OHC in 1966–1976 (short-dashed), 1978–1988 (solid), and 1989–1998 (long-dashed).

For the NINO3 index (Figure 3a), the low persistence (the dark shading) occurs near March before 1977, shifts to around July from 1978 to 1983, and shifts back to near April after 1990. The persistence barrier is relatively weak during 1978–1988 compared to other periods. It should be noted that in this period, a weaker secondary persistence barrier also appears in March. We also found a dramatic shift in the persistence for the OHC index (Figure 3b): The persistence barrier occurs near November–January before 1977, shifts to around April from 1978 to 1988, and shifts back to November–December afterward. We performed similar analyses with a 7-year and 15-year running window (not shown) and found little sensitivity of the results to the window length. On the basis of the near-decadal scale shifts, we divided the 1958–2001 period into three periods for further analysis: 1966–1976 (the first period, hereafter), 1978–1988 (the second period), and 1989–1998 (the third period). The second period is obviously the period when the ENSO persistence barriers in both the NINO3 and zonal mean OHC indices are most different from those of the other two periods. It is important to note that the decadal shifts of the barriers do not affect the phase lag between the SST and OHC barriers. In all three periods, the zonal mean OHC barrier leads the NINO3 SST barrier by about one season. This result implies that during the past four decades, the OHC information could always help overcome the NINO3 SST persistence barrier for better long-term predictions regardless of the shifts of the timing of their barriers. To make sure that the decadal changes shown in Figures 3a and b are not the results of the assimilation and reanalysis techniques used in the SODA and GISST products, we repeated the analysis to the ENACT-INGV OHC product and the ERSST V.2 SST data. The decadal barrier changes calculated from these two data sets (Figures 3c and d) are very similar to those shown in Figures 3a and b.

[10] We then linked the decadal changes of the persistence barriers to the ENSO properties in these three periods. Figure 4 shows the decadal variations of the variances of NINO3 SST and zonal mean OHC indices calculated from the SODA and GISST data sets. The variance is calculated within a 10-year window moving from 1958 to 2001. Figure 4a shows that the general ENSO SST intensity increases from the first period to the third period. The amplitudes in 1977–1987 and 1988–1998 are both larger than that in 1962–1976. Figure 4b shows that the OHC intensity is actually the largest in the second period. Therefore the decadal changes in the overall ENSO intensity are not responsible for the decadal changes of ENSO SST and OHC barriers. Previous studies suggested that the persistence barrier is caused by the phase locking of ENSO to the seasonal cycle [e.g., *Torrence and Webster*, 1998]. If, for example, ENSO events tend to start in spring, grow in summer and fall, reach maturity and largest amplitude in winter, SST anomalies are typically small in spring when the ENSO just transits from one phase (e.g., El Niño) to the other (e.g., La Niña). The small signal-to-noise ratio in the phase transition season makes ENSO anomalies easy to be disrupted by noise and results in weak persistence and, therefore, a spring barrier. To examine if it is the change of the phase locking that is responsible for the decadal barrier changes, we compare in Figure 5 the seasonal variations of the standard deviation of NINO3 and OHC indices in the three periods. For the NINO3 index (Figure 5a), the phase locking is the strongest in the first period with a maximum in December and a minimum in April that is consistent with the spring persistence barrier in that period. The third period also shows a similar seasonal variation in its NINO3 variance although the seasonal variation is not as strong as in the first period. In the second period, the seasonal variation of the SST standard deviation is the weakest among all the three periods. There are actually two local minima in the standard deviation: one in March–April and the other in July–August, consistent with the timing of the two weak persistence barriers shown in Figure 3a for this period. For the OHC index, the minimum values of its standard deviation occurred in winter (December–January) for both the first and the third periods but in near May in the second period. The timings are consistent with those of the OHC barriers shown in Figure 3b. The standard deviations calculated from the ENACT-INGV OHC and the ERSST V.2 SST exhibit similar seasonal variations (not shown). The consistency between Figures 3 and 5 indicates that the decadal changes of persistence barriers in both the NINO3

Table 1. Month of the Weakest Persistence

	NINO4	NINO3.4	NINO3	NINO1+2	Zonal-Mean OHC
1966–1976 (First period)	May	April	March	January	December
1978–1988 (Second period)	April–May	April–May	July	August	April
1989–1998 (Third period)	April	April	April	April	December

SST and the zonal mean OHC indices are caused by the changes in the phase locking of ENSO to the seasonal cycle.

4. Persistence Barriers in Other ENSO SST Indices

[11] We further expanded our analysis to three other ENSO SST indices: the NINO1+2, NINO3.4, and NINO4 indices, to determine if similar decadal barrier changes exist across the central-to-eastern equatorial Pacific. Figure 6 shows the decadal barrier variations of all the four NINO SST indices. The NINO3 barrier (Figure 3a) is reproduced here for the sake of comparison. It is interesting to notice from Figure 6 that the decadal barrier change is most obvious for the SST indices located closer to the eastern Pacific (NINO1+2 and NINO3) but becomes weak for the SST indices located toward the central Pacific (NINO3.4 and NINO4). The NINO3.4 index, for example, has its persistence barrier occurring always near April throughout the entire period of analysis, and the NINO4 index has its barrier mostly in April–May. Table 1 summaries the timing of the persistence barrier for the four SST indices. In the first period, the SST persistence barrier occurs in January for the NINO1+2 region, in March for the NINO3 region, in April for the NINO3.4 region, and in May for the NINO4 region, i.e., a westward migration of the timing of the persistence barrier. An eastward migration of the barrier can be identified in the second period during which the barrier appears first at the NINO3.4 and NINO4 regions in April–May, at the NINO3 region in July, and finally at the NINO1+2 region in August. In the third period, the barrier occurs almost simultaneously around April for all four NINO regions. Similar decadal barrier changes are found when the same analysis is applied to the ERSST V.2 SST data set (not shown). We also list in Table 1 the timing of the persistence barrier of the zonal mean OHC index. It

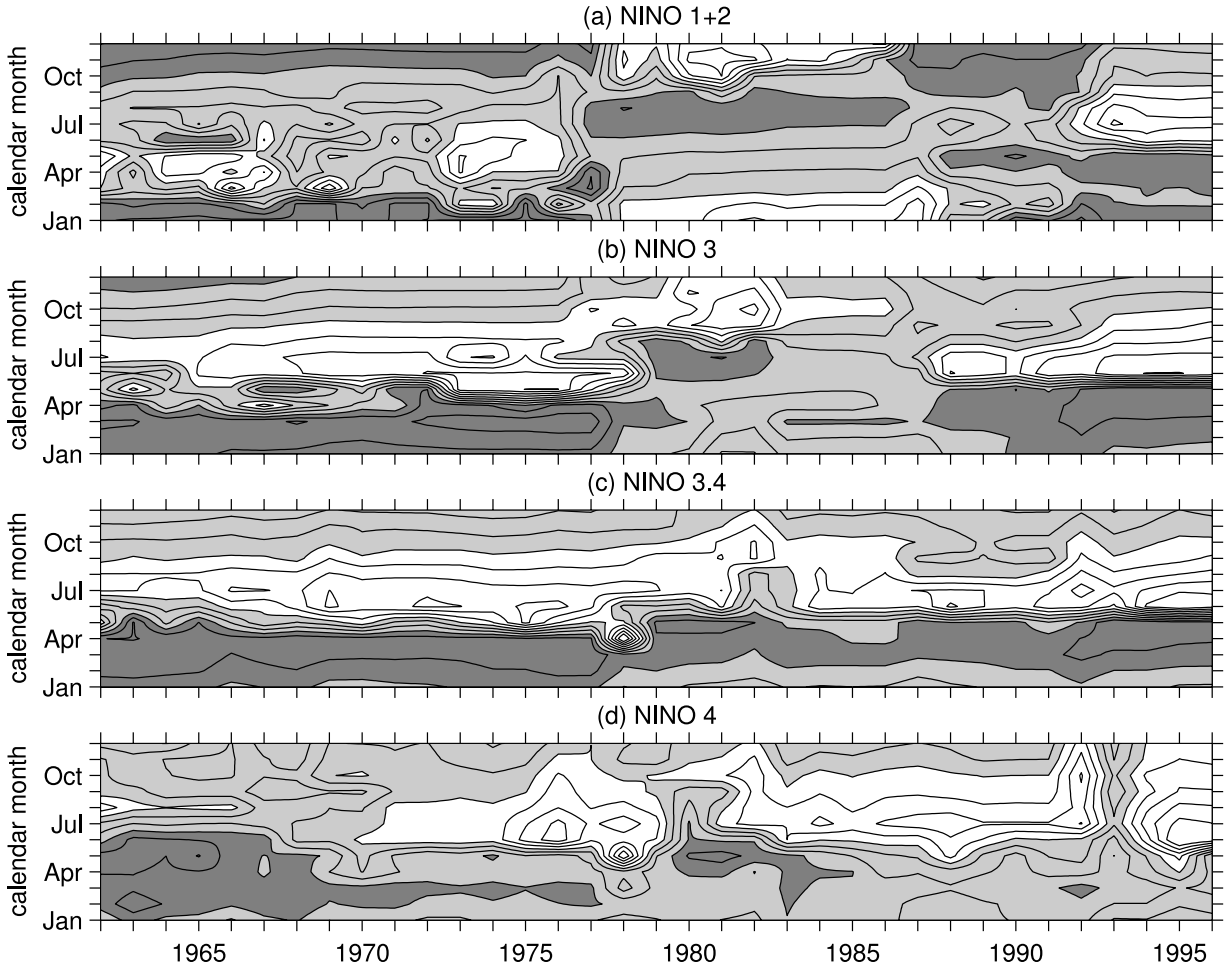

Figure 6. Same as Figure 3 except for (a) NINO1+2 SST index, (b) NINO3 SST index (same as Figure 3a), (c) NINO3.4 SST index, and (d) NINO4 SST index.

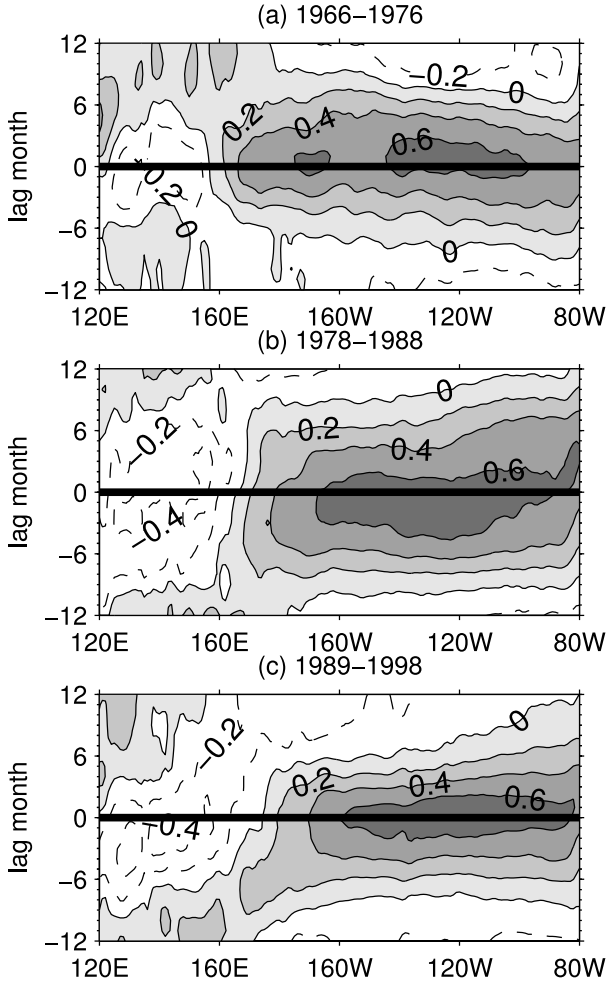

Figure 7. Lagged correlation coefficients between the NINO3 SST index and the SST anomalies along the equatorial Pacific (5°S to 5°N) during (a) 1966–1976, (b) 1978–1988, and (c) 1989–1998. Contour intervals are 0.2.

shows that the OHC index has a constant phase lag only with the NINO3 SST index in all three periods but not with the other NINO SST indices. This suggests that the evolution of mean equatorial Pacific OHC during ENSO is more closely linked to SST evolution in the NINO3 region.

[12] As explained in section 3, SST persistence barrier is caused by ENSO's phase locking to the seasonal cycle. The barrier occurs in the season when most of the phase transitions of ENSO events occur. The timing of the SST persistence barrier can therefore be used to infer the onset time of SST anomalies during ENSO events. On the basis of this view, the westward migration of the timing of the SST persistence barrier in the first period infers that the ENSO SST anomalies appeared first in the eastern Pacific and then in the central Pacific, i.e., a westward SST propagation pattern. Similarly, the ENSO SST propagation pattern should be eastward in the second period and almost standing in the third period. These SST propagation patterns are confirmed by Figure 7 in which we show the lagged correlation coefficients between the NINO3 SST index and the SST anomalies along the equatorial Pacific for the three periods. In 1966–1976 (Figure 7a), ENSO SST anomalies start in the far eastern Pacific and propagate westward toward the central Pacific. In 1978–1988 (Figure 7b), ENSO SST anomalies appear first near the central Pacific and then extend eastward toward the eastern Pacific. In 1989–1998 (Figure 7c), the anomalies appear almost the same time across the central-to-eastern Pacific. The changes of ENSO SST propagation patterns before and after the 1970s are consistent with those reported by earlier studies [e.g., *Wang*, 1995]. Our results further show that the propagation pattern changes again in the 1990s. In addition, this study shows that the changes of the ENSO SST propagation pattern are related to the different decadal changes of SST persistence barrier between the eastern and the central equatorial Pacific. It is important to note that the persistence barriers in the central equatorial Pacific (the NINO3.4 and NINO4 regions) are locked to April–May no matter whether the SST anomalies propagate eastward or westward. It suggests that the physical process that controls the phase transition of SST anomalies in the central Pacific may be different from the one that controls the SST phase transition in the eastern Pacific. If the latter process produces an SST transition earlier than April, the ENSO events will appear propagating westward. If the transition occurs later than April, the ENSO events will appear propagating eastward. Therefore the propagation pattern of ENSO SST anomalies does not have to be explained as a result of a single air-sea interaction process that continuously shifts SST anomalies eastward or westward [*Neelin*, 1991].

5. Changes in the Oceanic and Atmospheric Basic States

[13] It has been shown by *Fedorov and Philander* [2000] that the ENSO dynamics depends on the mean thermocline depth and trade wind strength over the equatorial Pacific. In this section, we examined the decadal changes of these two quantities to understand their linkages to the 1976/1977 and 1989/1990 shifts of the persistence barriers. Figure 8a shows the annual mean values of the equatorial Pacific OHC (averaged between 5°S and 5°N and between 120°E and 80°W) from 1958 to 2001. A 5-year running mean is applied to the time series to retain only the slow evolution part of the time series. A major feature in this figure is a rapid shift of the mean OHC from a warmer OHC state (and therefore a deeper thermocline) before the 1980s to a colder state (a shallower thermocline) afterward. The rapid shift began near the late 1970s and ended near the late 1980s, a period that coincides with the second period (1978–1988) of the decadal ENSO barrier change. The OHC variation implies that the mean equatorial Pacific thermocline stayed at a deeper depth in the first period (1966–1976), shifted upward quickly during the second period, and reached and stayed at a shallower depth in the third period (1989–1998). ENSOs in the first and third periods were produced with more-or-less fixed mean thermocline depths, while ENSOs in the second period were produced with an evolving mean thermocline. The ENSO dynamics and therefore the persistence barrier in the second period are different from those in the other periods. To verify the OHC shift, we also analyzed the annual mean OHC values from the ENACT-INGV ocean analysis and the upper ocean temperature compiled by the

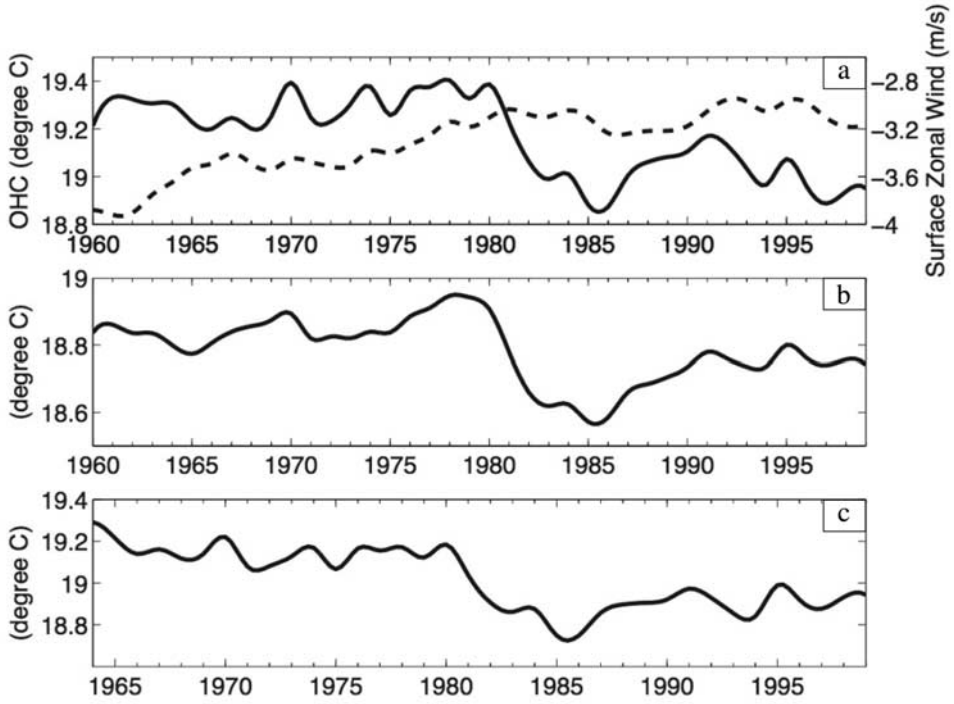

Figure 8. Annual means of equatorial Pacific OHC (5°S–5°N; 120°E–80°W) calculated from (a) the SODA data (solid), (b) the JEDAC data and (c) the ENACT INGV data. Annual means of surface zonal wind calculated from ERA-40 (dashed) are also shown in Figure 8a. A 5-year running is applied.

Joint Environmental Data Analysis Center (JEDAC) [*White and Bernstein*, 1979]. The JEDAC data set is derived from the upper ocean temperatures observed by mechanical bathythermograph. The data we downloaded from JEDAC cover 1955 to 2003. Both the ENACT-INGV (Figure 8b) and the JEDAC (Figure 8c) data sets show dramatic shifts in the mean equatorial Pacific OHC before and after 1976/1977 similar to the SODA data.

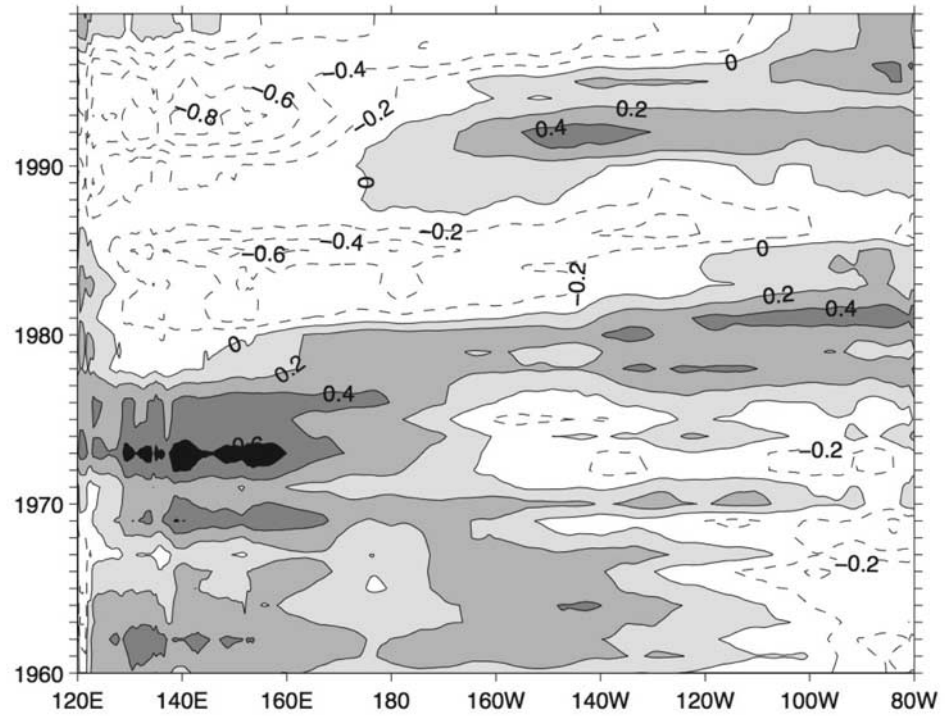

Figure 9. Deviations of annual mean OHC value of the equatorial Pacific (5°S–5°N) from its long-term mean. Contour intervals are 0.2°C.

[14] The east-west slope of the thermocline affects the coupling strength between the atmosphere and the ocean and is important to determine ENSO activities. Figure 9 displays the deviations of the annual mean Pacific OHC from its long-term (1958–2001) mean in the SODA data. A 5-year running mean is also applied in this figure. It is clear from the figure that the OHC in both the eastern and the western equatorial Pacific experienced rapid shifts during 1978–1986. The OHC shifted to larger values in the eastern Pacific but to smaller values in the western Pacific. That means that the thermocline depth became deeper in the eastern Pacific but shallower in the western Pacific after the shift. As a result, the equatorial thermocline has a larger slope before 1977/1978 but has a smaller slope afterward. In consistence with the changes in the thermocline slope, the easterlies were weakened in the central Pacific after the 1970s (see Figure 8a). The basic state changes apparently affect the eastern Pacific SST barriers but not the central Pacific SST barriers. This suggests that the physical process controlling SST evolution and persistence barrier in the eastern Pacific is an atmosphere-ocean coupling process which is affected by the decadal variation of the thermocline depth. On the other hand, the physical process controlling SST evolution and barrier in the central Pacific is not related to the thermocline variation. As a result, when the equatorial Pacific thermocline depth changes, the decadal barrier change is large in the eastern Pacific but small in the central Pacific.

6. Conclusions and Discussions

[15] In this study we analyzed the decadal changes of ENSO persistence barrier in various SST and OHC indices during 1958–2001. One major finding is that both the ENSO SST and the OHC indices exhibit dramatic shifts near 1976/1977 and 1989/1999 in the timing of their persistence barriers. This finding adds another evidence to the assertion that significant climate shifts occurred in the Pacific not only in 1977 but also in 1990 [*Hare and Mantua*, 2000]. We found that the phase lag between the SST and the OHC barriers remain fixed throughout the last four decades, indicating that OHC information should be always useful in overcoming the spring barrier of SST for ENSO prediction. Another major finding of this study is that the decadal changes of SST barrier are much larger in the eastern equatorial Pacific than in the central equatorial Pacific. The SST barriers in the eastern Pacific (NINO1+2 and NINO3 regions) shifted dramatically near the late 1970s and again in the late 1980s, which coincided with the decadal changes of the mean thermocline depth along the equatorial Pacific. In contrast, the basic state changes do not affect the SST barrier in the central Pacific (NINO3.4 and NINO4 regions) which remained fixed in mid-spring throughout the past four decades. These results suggest that ENSO SST anomalies in the equatorial Pacific may be considered as consisting of two different processes: a central Pacific process which is strongly phase-locked to the seasonal cycle and always starts in spring, and an eastern Pacific process whose onset timing changes from decade to decade and is related to changes in the mean state of the ocean. This view of ENSO has to be further examined with simple model experiments.

[16] It is interesting to mention that the decadal SST barrier changes found in this study can be used to explain the decadal changes in the retrospective ENSO predictions reported in the study of *Ji et al.* [1996]. They used three different versions of National Centers for Environmental Prediction coupled general circulation model (CGCM) to perform 6-month hindcasts of ENSO events from 1982 to 1995. They found the prediction more successful for the ENSOs in the 1980s than the ENSOs in the 1990s. This is consistent with our Figure 3a that the SST barrier tends to be weaker in the 1980s than in the 1990s. More interestingly, they found that their CGCMs have higher prediction skills in the central Pacific for the prediction of winter ENSO SST anomalies and higher skills in the eastern Pacific for the summer SST prediction (see their Figures 4 and 5). These different skills can be explained by the different decadal SST barriers we found in Figure 6. The period that they studied, 1982–1995, falls mostly within the second period of our study. In this period, Figure 6 shows that the SST persistence barrier occurs at July–August in the eastern Pacific and at March–April in the central Pacific. For the 6-month hindcasts of winter SSTs, the predictions run across the July–August SST barrier in the eastern Pacific and should have a low prediction skill in the eastern Pacific but a high skill in the central Pacific. Similarly, their summer predictions encounter the March–April SST barrier in the central Pacific and should show a low prediction skill there but a high skill in the eastern Pacific. This example demonstrates that much can be learned on the decadal changes of ENSO predictability from the analyses presented in this study.

[17] **Acknowledgments.** The authors thank the anonymous reviewers for their suggestions on the improvements of this paper. The authors benefit from the discussion with Dr. Tong Lee of JPL. The research was supported by NSF (ATM-0638432) and NASA (NNX06AF49H) grants. Data analyses were performed at the University of California Irvine's Earth System Modeling Facility and the San Diego Supercomputer Center. The SODA data are downloaded from http://iridl.ldeo.columbia.edu/SOURCES/.CARTON-GIESE/SODA/, the JEDAC data from http://coaac.ucsd.edu/DATA_IMAGES/index.html, the GISST data from http://hadobs.metoffice.com/hadisst/data/download.html, and the NOAA_ERSST V.2 from http://www.cdc.noaa.gov/.

References

An, S.-I., and B. Wang (2000), Interdecadal change of the structure of the ENSO mode and its impact on the ENSO frequency, *J. Climate*, *13*, 2044–2055.

Balmaseda, M. A., M. K. Davey, and D. L. T. Anderson (1995), Decadal and seasonal dependence of ENSO prediction skill, *J. Climate*, *8*, 2705–2715.

Barnston, A. G., et al. (1994), Long-lead seasonal forecasts: where do we stand?, *Bull. Am. Meteorol. Soc.*, *75*, 2097–2114.

Carton, J. A., G. Chepurin, and X. Cao (2000a), A simple ocean data assimilation analysis of the global upper ocean 1950–95. Part I: Methodology, *J. Phys. Oceanogr.*, *30*, 294–309.

Carton, J. A., G. Chepurin, and X. Cao (2000b), A simple ocean data assimilation analysis of the global upper ocean 1950–95. Part II: Results, *J. Phys. Oceanogr.*, *30*, 311–326.

Chen, D., S. E. Zebiak, A. J. Busalacchi, and M. A. Cane (1995), An improved procedure for El Niño forecasting, *Science*, *269*, 1699–1702.

Clarke, A. J., and S. Van Gorder (1999), The connection between the boreal spring southern oscillation persistence barrier and biennial variability, *J. Climate*, *12*, 610–620.

Fedorov, A. V., and S. G. Philander (2000), Is El Niño changing?, *Science*, *288*, 1997–2002.

Gu, D., and S. G. H. Philander (1995), Secular changes of annual and interannual variability in the tropics during the past century, *J. Climate*, *8*, 864–876.

Hare, S. R., and N. J. Mantua (2000), Empirical evidence for North Pacific regime shifts in 1977 and 1989, *Prog. Oceanogr.*, *47*, 104–145.

Ji, M., A. Leetmaa, and V. E. Kousky (1996), Coupled model predictions of ENSO during the 1980s and the 1990s at the National Centers for Environmental Prediction, *J. Climate*, *9*, 3105–3120.

Latif, M., D. Anerson, T. P. Barnett, M. A. Cane, R. Kleeman, A. Leetmaa, J. J. O'Brien, A. Rostati, and E. K. Schneider (1998), A review of predictability and prediction of ENSO, *J. Geophys. Res.*, *103*, 14,375–14,394.

Madec, G., P. Delecluse, M. Imbard, and C. Lévy (1998), OPA 8.1 Ocean General Circulation Model reference manual. Note du Pôle de modélisation, Institut Pierre-Simon Laplace, N°11, 91 pp.

McPhaden, M. J. (2003), Tropical Pacific Ocean heat content variations and ENSO persistence barriers, *Geophys. Res. Lett.*, *30*(9), 1480, doi:10.1029/2003GL016872.

Neelin, J. D. (1991), The slow sea surface temperature mode and the fast-wave limit: Analytic theory for tropical interannual oscillations and experiments in a hybrid coupled model, *J. Atmos. Sci.*, *48*, 584–606.

Rayner, N. A., E. B. Horton, D. E. Parker, C. K. Folland, and R. B. Hackett (1996), Version 2.2 of the Global Sea-Ice and Sea Surface Temperature data set, Climate Research Technical Note, 1903–1994, CRTN 74, Hadley Centre for Climate Prediction and Research, Meteorological Office, Bracknell, UK.

Smith, T. M., and R. W. Reynolds (2004), Improved extended reconstruction of SST (1854–1997), *J. Climate*, *17*, 2466–2477.

Torrence, C., and P. J. Webster (1998), The annual cycle of persistence in the El Niño-Southern Oscillation, *Q. J. R. Meteorol. Soc.*, *124*, 1985–2004.

Troup, A. J. (1965), The "southern oscillation", *Q. J. R. Meteorol. Soc.*, *91*, 490–506.

Uppala, S., J. K. Gibson, M. Fiorino, A. Hernandez, P. Kallberg, X. Li, K. Onogi, and S. Saarinen (1999), ECMWF's Second Generation Reanalysis—ERA-40, Proceedings of the Second International Conference on Reanalyses, Wokefield Park, Mortimer, Reading, UK, 23–28 August.

Wang, B. (1995), Interdecadal changes in El Niño onset in the last four decades, *J. Climate*, *8*, 267–285.

Webster, P. J., and S. Yang (1992), Monsoon and ENSO: Selectively interactive systems, *Q. J. R. Meteorol. Soc.*, *118*, 877–925.

Weiss, J. P., and Jeffrey B. Weiss (1999), Quantifying persistence in ENSO, *J. Atmos. Sci.*, *56*, 2737–2760.

White, W. B., and R. L. Bernstein (1979), Design of an oceanographic network in the mid-latitude North Pacific, *J. Phys. Oceanogr.*, *9*, 592–606.

Wright, P. B. (1979), Persistence of rainfall anomalies in the central Pacific, *Nature*, *277*, 371–374.

Xue, Y., A. Leetmaa, and M. Ji (2000), ENSO prediction with Markov models: The impact of sea level, *J. Climate*, *13*, 849–871.

H.-Y. Kao and J.-Y. Yu, Department of Earth System Science, University of California, Irvine, CA 92697-3100, USA. (jyyu@uci.edu)